

Quantum Monte Carlo study of the one-dimensional Holstein model of spinless fermions

Ross H. McKenzie*, C. J. Hamer, and D. W. Murray
School of Physics, University of New South Wales, Sydney 2052, Australia
(Received 29 November 1995)

The Holstein model of spinless fermions interacting with dispersionless phonons in one dimension is studied by a Green's function Monte Carlo technique. The ground state energy, first fermionic excited state, density wave correlations, and mean lattice displacement are calculated for lattices of up to 16 sites, for one fermion per two sites, i.e., a half-filled band. Results are obtained for values of the fermion hopping parameter of $t = 0.1\omega$, ω , and 10ω where ω is the phonon frequency. At a finite fermion-phonon coupling g there is a transition from a metallic phase to an insulating phase in which there is charge-density-wave order. Finite size scaling is found to hold in the metallic phase and is used to extract the coupling dependence of the Luttinger liquid parameters, u_ρ and K_ρ , the velocity of charge excitations and the correlation exponent, respectively. For free fermions ($g = 0$) and for strong coupling ($g^2 \gg t\omega$) our results agree well with known analytic results. For $t = \omega$ and $t = 10\omega$ our results are inconsistent with the metal-insulator transition being a Kosterlitz-Thouless transition.

To appear in Physical Review B, April 15, 1996.

PACS numbers:71.38.+i, 02.70.Lq, 71.45.Lr, 71.30.+h, 63.20.Kr

I. INTRODUCTION

A wide range of quasi-one-dimensional materials have electronic properties that are dominated by the Peierls or charge-density-wave instability caused by the electron-phonon interaction¹. For a half-filled band it is energetically favourable for the lattice to dimerize and open an energy gap at the Fermi surface. Although the lattice distortion increases the lattice energy, opening the electronic energy gap preferentially lowers the total energy for highly anisotropic systems². These systems are often modelled by the one-dimensional Holstein³ or Su-Schrieffer-Heeger (SSH)⁴ models. Most treatments of the Peierls instability treat the phonons in the mean-field or rigid lattice approximation. This is questionable in one-dimension and furthermore, in a wide-range of materials the lattice distortion is comparable to the zero-point motion of the lattice⁵. It has recently been shown that the quantum lattice fluctuations must be taken into account to satisfactorily describe optical properties^{6,7}. Several authors have previously considered the role of quantum lattice fluctuations for the SSH model⁸ and the Holstein model⁹⁻¹² at half-filling. Voit and Schulz have considered the interplay of quantum lattice fluctuations and electron-electron interactions away from half-filling¹³. Recently the Holstein model, also known as the molecular crystal model, has received considerable attention because the challenge of high- T_c and fullerene superconductors has revealed deficiencies in our understanding of the electron-phonon interaction and the competition between superconductivity and charge-density-wave instabilities. This has motivated studies of the Holstein model in infinite dimensions¹⁴, two dimensions¹⁵, one dimension¹⁶ and on just a few sites¹⁷.

We consider the Holstein model in one dimension at half filling and only with spinless fermions, for simplicity. The spinless fermions hop along a one-dimensional chain and interact with a phonon mode located on each lattice site. The creation operator for a fermion on site i is denoted c_i . The fermions can hop between neighbouring sites with amplitude t . In the absence of interactions the phonons all have the same frequency ω , i.e., they are dispersionless. The electron-phonon coupling, in units of energy, is g . Phonon position and momentum operators are denoted by q_i and p_i , respectively. The Hamiltonian for the Holstein model (at half filling) is⁹

$$H = -t \sum_i \left(c_i^\dagger c_{i+1} + c_{i+1}^\dagger c_i \right) - g(2M\omega)^{1/2} \sum_i \left(c_i^\dagger c_i - \frac{1}{2} \right) q_i + \sum_i \frac{1}{2M} p_i^2 + \frac{1}{2} M \omega^2 q_i^2 - \frac{N}{2} \omega \quad (1)$$

for a system of N lattice sites. This Hamiltonian has particle-hole symmetry since the transformation $c_i \rightarrow (-1)^i c_i^\dagger$, $q_i \rightarrow -q_i$ leaves H invariant. This discrete symmetry is broken in the charge-density-wave phase which has the electronic order parameter

$$m_e \equiv \frac{1}{N} \sum_i (-1)^i \langle c_i^\dagger c_i \rangle \quad (2)$$

and the phonon order parameter

$$m_p \equiv \frac{1}{N} \sum_i (-1)^i \langle q_i \rangle \quad (3)$$

which is a measure of the dimerization.

If phonon creation and annihilation operators are denoted by a_i^\dagger and a_i , respectively, the Hamiltonian (1) can be written

$$H = -t \sum_i \left(c_i^\dagger c_{i+1} + c_{i+1}^\dagger c_i \right) - g \sum_i \left(c_i^\dagger c_i - \frac{1}{2} \right) \left(a_i + a_i^\dagger \right) + \omega \sum_i a_i^\dagger a_i. \quad (4)$$

Thus ground state properties will be determined by two independent parameters, which we will take to be t/ω and g/ω . It is also useful to define the dimensionless electron-phonon coupling

$$\lambda \equiv \frac{g^2}{\pi t \omega}. \quad (5)$$

Although for simplicity we confine ourselves to the case of spinless fermions this model is still of physical relevance in at least two situations. The first situation concerns strongly correlated electron systems. In the infinite U limit the Hubbard model is known to map onto the case of spinless fermions¹⁸. This may be realized in the 1:2 TCNQ salts¹⁹. The second situation concerns the spin-Peierls transition²⁰. Using a Jordan-Wigner transformation²¹ this model can be mapped onto a XX spin chain in zero field with the Hamiltonian:

$$H = -2t \sum_i \left(S_i^x S_{i+1}^x + S_i^y S_{i+1}^y \right) - g \sum_i S_i^z \left(a_i + a_i^\dagger \right) + \omega \sum_i a_i^\dagger a_i. \quad (6)$$

It should be pointed out that this is not the standard Hamiltonian used to study the spin-Peierls transition. However, it does have the same qualitative features: i.e., a dimerization of the phonons results in a spin singlet ground state with an energy gap.

It was recently shown²² rigorously that for the one-dimensional Holstein model of spinless fermions at half-filling there is no long range order for sufficiently small coupling g . Hirsch and Fradkin⁹ studied the Holstein model at half-filling using a world-line Monte Carlo technique and a strong coupling expansion. The expansion suggested that for spinless fermions quantum lattice fluctuations destroy the dimerized state if the fermion-phonon coupling was sufficiently weak and the phonon frequency sufficiently high. The quantum Monte Carlo simulations were performed for $0.5\omega < t < 3\omega$ and gave a phase diagram qualitatively consistent with the strong coupling expansion. In contrast, for fermions with spin their results were consistent with dimerization for finite phonon frequency and all non-zero couplings.

Zheng, Feinberg, and Avignon¹¹ used a variational polaron wave function to study the Holstein model at half-filling. For spinless fermions the ground state is a charge-density wave for *all* parameter values. Most of their results were consistent with Hirsch and Fradkin. However, they found that for large phonon frequencies ($t > 0.3\omega$) there was a first-order phase transition, with a very large jump in the CDW order parameter, between CDW phases when $g^2 \sim 10\omega$. They point out that this transition may be an artefact of the variational treatment since it is known that in small-polaron theory of a single electron a similar two-minimum structure, leading to non-analytic behaviour sometimes referred to as “self-trapping,” occurs and is known to be an artefact of the variational treatment^{23,24}.

This paper presents a study of the Holstein model using a Green’s Function Monte Carlo technique. Section II reviews how the metallic phase should be a Luttinger liquid and how finite-size scaling can be used to extract the Luttinger liquid parameters. Section III briefly summarizes known analytic results of the Holstein model that can be used to check and help understand our Monte Carlo results. Section IV contains a detailed description of the Green’s Function Monte Carlo technique that we use. Our results are presented and interpreted in Section V. The physical picture that emerges from our results is discussed in the final section.

II. LUTTINGER LIQUIDS AND FINITE-SIZE SCALING

A. The Luttinger liquid conjecture

For weak coupling and high frequency the system is in a metallic, i.e., gapless phase. According to Haldane's "Luttinger liquid" conjecture^{18,25} this phase should be in the same universality class as the Tomonaga-Luttinger model of interacting spinless fermions. This means the low-energy properties of the metallic phase are completely described by an effective Luttinger model with two parameters u_ρ , the velocity of charge excitations or renormalized Fermi velocity, and K_ρ , the renormalized effective coupling (stiffness) constant. Important properties of the Luttinger model, quite distinct from those of a conventional Fermi liquid, are (i) there are no quasi-particle excitations at the Fermi surface and (ii) all correlation functions have non-universal exponents that can be written in terms of the single parameter K_ρ . For example, K_ρ determines the singularity of the momentum distribution function close to the Fermi surface²⁶:

$$n(k) \simeq \frac{1}{2} - \text{sign}(k - k_F)|k - k_F|^\alpha \quad (7)$$

and of the single-particle density of states

$$\rho(E) \sim |E|^\alpha \quad (8)$$

where

$$\alpha \equiv \frac{1}{2}(K_\rho + \frac{1}{K_\rho} - 2). \quad (9)$$

For free fermions $K_\rho = 1$ and $\alpha = 0$. For attractive (repulsive) interactions $K_\rho > 1$ ($K_\rho < 1$). It is remarkable that, as explained below, the parameters u_ρ and K_ρ can be determined from numerical calculations on systems of finite size.

B. Finite size scaling

The ground state energy $E_0(N)$ of a conformally invariant system of N sites is, to leading order in $1/N$ ²⁷,

$$\frac{E_0(N)}{N} = \epsilon_\infty - \frac{\pi u_\rho C}{6N^2} \quad (10)$$

where ϵ_∞ is the ground state energy per site of the infinite system, u_ρ is the velocity of charge excitations, and C is the conformal charge. Care must be taken with boundary conditions. We use anti-periodic (periodic) boundary conditions for the fermions when there is an even (odd) number of fermions. This corresponds to periodic boundary conditions for the associated spin or bosonic models²¹. If the system is a Luttinger liquid it belongs to the same universality class as the Gaussian model and $C = 1$ ¹⁸. The slope of a plot of $E_0(N)/N$ versus $1/N^2$ (compare Figure 1) can then be used to determine u_ρ .

The energy of the first excited state is, to leading order in $1/N$,

$$E_1(N) - E_0(N) = \frac{2\pi u_\rho x}{N} \quad (11)$$

where x is the scaling dimension²⁸. A Luttinger liquid has the unusual property that x depends on the coupling constants.

In the presence of particle-hole symmetry x can be related to the correlation exponent K_ρ which determines the asymptotic decay of *all* correlation functions. Let $E_{\pm 1}(N)$ denote the ground state energy of $N/2 \pm 1$ fermions on N sites. By particle-hole symmetry $E_{+1}(N) = E_{-1}(N)$. In a general Luttinger liquid of spinless fermions¹⁸ with charge density n the compressibility κ is given by

$$\frac{1}{n^2 \kappa} \equiv \frac{\partial^2 \epsilon_\infty(n)}{\partial n^2} = \frac{\pi u_\rho}{K_\rho} \quad (12)$$

Since particle-hole symmetry implies $\frac{\partial \epsilon_\infty(n)}{\partial n} = 0$ it follows that

$$E_{\pm 1}(N) = E_0(N) + \frac{1}{2} \left(\frac{1}{N} \right)^2 N \frac{\partial^2 \epsilon_\infty(n)}{\partial n^2} \quad (13)$$

which with (12) implies that to leading order in $1/N$

$$E_{\pm 1}(N) - E_0(N) = \frac{\pi u_\rho}{2K_\rho N} \quad (14)$$

This is identical to (11) with $K_\rho = 1/4x$. Hence, if u_ρ is known a plot of the energy gap versus $1/N$ (compare Figure 2) can be used to determine K_ρ .

III. ANALYTIC RESULTS

Certain limits of the Holstein model for which analytic results can be obtained are now briefly reviewed. These results will be compared to the appropriate numerical results.

A. Localized fermions ($t = 0$)

The fermions cannot move between sites and the Hamiltonian reduces to N independent Hamiltonians. The Hamiltonian for the i th site is

$$H_i = \frac{1}{2M} p_i^2 + \frac{1}{2} M \omega^2 q_i^2 - (n_i - \frac{1}{2}) g (2M\omega)^{1/2} q_i - \frac{1}{2} \omega \quad (15)$$

where $n_i \equiv c_i^\dagger c_i$ is the fermion occupation at site i . The presence or absence of a fermion shifts the equilibrium position of the oscillator to $+q_e$ or $-q_e$, respectively, where

$$q_e = g \left(\frac{M}{2\omega} \right)^{\frac{1}{2}} = \langle q_i (2n_i - 1) \rangle \quad (16)$$

This Hamiltonian can be diagonalized by the Lang-Firsov transformation²⁹: $c_i \rightarrow c_i \exp(q_e(a_i^\dagger - a_i))$, $a_i \rightarrow a_i - (2n_i - 1)q_e$. The mean square lattice displacement is

$$\langle q_i^2 \rangle = q_e^2 + \frac{1}{2M\omega}. \quad (17)$$

The ground state energy per site is

$$\epsilon_\infty = -\frac{g^2}{4\omega}. \quad (18)$$

B. Small Polarons ($g^2 \gg t\omega$)

This corresponds to the case of a narrow band of small polarons³. The intersite hopping represents a small perturbation on the situation considered in the previous section. Hirsch and Fradkin⁹ derived an effective Hamiltonian³⁰ involving the new fermion operator C_i^\dagger that creates a fermion at site i and changes the oscillator ground state from one centered at $-q_e$ to one centered at $+q_e$.

$$H_{eff} = -N \frac{g^2}{4\omega} - J \sum_i \left(C_i^\dagger C_{i+1} + C_{i+1}^\dagger C_i \right) + V \sum_i \left(C_i^\dagger C_i - \frac{1}{2} \right) \left(C_{i+1}^\dagger C_{i+1} - \frac{1}{2} \right) \quad (19)$$

The first term is the polaron binding energy (compare equation (18)) and dominates the ground state energy (Figure 3). The second term describes hopping between neighbouring sites with the bandwidth reduced by the overlap of the oscillator ground state centered at $-q_e$ and $+q_e$:

$$J = t \exp \left(- \left(\frac{g}{\omega} \right)^2 \right). \quad (20)$$

The third term describes the second order process (of order t^2/ω) where a fermion hops to a neighbouring site and back again. This term is repulsive because this process is not possible if the neighbouring site is occupied.

$$V = \frac{2J^2}{\omega} \int_0^{(g/\omega)^2} dx \frac{e^{2x} - 1}{x} \quad (21)$$

There is an additional term, of second order in t^2/ω , involving next nearest neighbour interactions but it is smaller by a factor of order $1/\lambda$ and so the effective Hamiltonian should accurately describe the physics in the strong coupling limit, $\lambda \gg 1$ or $g^2 \gg t\omega$. Note that the limit $\omega \rightarrow \infty$ corresponds to free fermions, as pointed out by Hirsch and Fradkin⁹.

The effective Hamiltonian (19) is, after a Jordan Wigner transformation, of the same form as that of the exactly soluble antiferromagnetic XXZ quantum spin chain²¹. For convenience we now briefly summarize some of the known results for this model. It can be exactly solved by Bethe ansatz^{31,32}. The system is metallic for $V < 2J$, i.e., there is no energy gap or long range order and so it is a Luttinger liquid. It is in an insulating charge-density-wave state for $V > 2J$. The metal-insulator transition is an infinite order, i.e. Kosterlitz-Thouless, transition and has been discussed in detail by Shankar³³.

Define a new variable μ by

$$\cos \mu = \frac{V}{2J} \quad (22)$$

where $0 < \mu < \pi/2$. As V increases from 0 to the transition at $V = 2J$, μ decreases from $\pi/2$ to zero. The velocity of charge excitations is given by²⁵

$$u_\rho = \pi J \frac{\sin \mu}{\mu}. \quad (23)$$

As V increases from 0 to the transition at $V = 2J$, the velocity increases from $2J$ to πJ . However, as the coupling g increases J rapidly decreases and so u_ρ rapidly decreases (compare Figure 4 (a)). The Luttinger liquid exponent K_ρ is

$$K_\rho = \frac{1}{2(1 - \frac{\mu}{\pi})}. \quad (24)$$

As V increases from 0 to the transition at $V = 2J$, K_ρ decreases from 1 to 1/2 (compare Figure 4 (b)). The value $K_\rho = 1/2$ is a universal feature of a Kosterlitz-Thouless transition for one-dimensional fermions^{33,34}.

For V larger than $2J$ define a new variable γ by

$$\cosh \gamma = \frac{V}{2J}. \quad (25)$$

The charge-density-wave order parameter (2) is³⁵

$$m_e = \frac{1}{2} \prod_{m=1}^{\infty} \tanh^2(m\gamma). \quad (26)$$

The coupling dependence is shown in Figure 5 (a) for $t = 0.1\omega$. The metal-insulator transition is Kosterlitz-Thouless although it does not appear so on the scale shown. The energy gap in the insulating phase is

$$\Delta = 2J \sinh \gamma \sum_{m=-\infty}^{m=\infty} \frac{(-1)^m}{\cosh(m\gamma)} \quad (27)$$

and turns out to be very small (compare Figure 5 (b)).

C. Free fermions ($g = 0$)

The fermion states are plane waves with energy dispersion

$$E(k) = -2t \cos(k). \quad (28)$$

These states are occupied for $|k| < k_F \equiv \pi/2$. Near the Fermi surface at $k = \pm k_F$ we have $E(k) = \pm 2t(k \mp k_F)$ and so the Fermi velocity is $v_F = 2t$. The ground state energy per site is

$$\epsilon_\infty = -2t \int_{-\pi/2}^{\pi/2} \frac{dk}{2\pi} \cos(k) = -\frac{2t}{\pi}. \quad (29)$$

D. Adiabatic or mean-field limit ($\omega \ll te^{-1/\lambda}$)

It is assumed that the fluctuations of the lattice about its dimerized value can be neglected and the quantum operator q_i in the Hamiltonian (1) is replaced by its mean value: $q_i \rightarrow \langle q_i \rangle = (-1)^i m_p$. The fermionic Hamiltonian can then be diagonalized by a Bogoliubov transformation and the fermionic energies are

$$E(k) = \pm \left((2t \cos(k))^2 + \Delta^2 \right)^{\frac{1}{2}} \quad (30)$$

where $\Delta \equiv g(2M\omega)^{1/2}m_p$ is the energy gap at the Fermi surface due to the dimerization. Δ is then treated as a variational parameter and the total energy of the system is minimized to give the self consistent equation

$$1 = \lambda t \int_{-\pi/2}^{\pi/2} dk \frac{1}{\left((2t \cos(k))^2 + \Delta^2 \right)^{\frac{1}{2}}}. \quad (31)$$

The system is dimerized for all coupling strengths and for weak coupling ($\lambda < 1$) the energy gap is

$$\Delta = 8t \exp\left(\frac{-1}{\lambda}\right). \quad (32)$$

The charge-density-wave order parameter is

$$m_e = \frac{\Delta}{2\pi\lambda t} = \frac{4}{\pi\lambda} \exp\left(\frac{-1}{\lambda}\right). \quad (33)$$

The corrections to the mean-field equation (31), to next order in $\omega\lambda/\Delta$, were recently calculated¹².

IV. THE GREEN'S FUNCTION MONTE CARLO METHOD

At first we tried simulating the model using a discrete basis of free phonon eigenstates on each site and employing a ‘‘stochastic truncation’’³⁶ technique appropriate to this basis. This method gave accurate results for small coupling g , but not at or beyond the metal-insulator transition. In this region the staggered displacement m_p becomes large, corresponding to the presence of highly excited states in the free phonon eigenstate basis. It was thus found more appropriate to use a continuous ‘‘position space’’ basis with variables $\{q_i\}$, and use a different Monte Carlo technique as described below.

A. Ground state energy

To simulate the model, we use a Green’s Function Monte Carlo (GFMC) method, as developed by Kalos and collaborators^{37,38}, and applied to lattice gauge theory by Chin, Negele and Koonin³⁹ and others^{40–42}. Let us review the method briefly.

The Hamiltonian for the Holstein model (1) can be rescaled to the dimensionless form

$$H = -\tilde{t} \sum_i \left(c_i^\dagger c_{i+1} + c_{i+1}^\dagger c_i \right) + \sum_i p_i^2 + q_i^2 - \tilde{g} q_i \left(n_i - \frac{1}{2} \right) \quad (34)$$

where $\tilde{t} \equiv 2t/\omega$, $\tilde{g} \equiv 2\sqrt{2}g/\omega$. The imaginary-time Schrodinger equation for the system reads

$$-\frac{\partial}{\partial \tau} |\Phi(\tau)\rangle = (H - E_T) |\Phi(\tau)\rangle \quad (35)$$

where E_T is a trial energy, representing a constant shift in the zero of energy. Evolving this equation for time $\Delta\tau$ yields

$$|\Phi(\tau + \Delta\tau)\rangle = \exp(\Delta\tau(E_T - H)) |\Phi(\tau)\rangle. \quad (36)$$

At large times τ the ground state will dominate:

$$|\Phi(\tau)\rangle \sim c_0 \exp(-(E_0 - E_T)\tau) |\Phi_0\rangle \quad \text{as } \tau \rightarrow \infty \quad (37)$$

where $|\Phi_0\rangle$ is the (time-independent) ground state of H with energy E_0 .

We shall work in a position-space representation, where the wave function

$$\Phi(\{q, n\}, \tau) = \langle \{q, n\} | \Phi(\tau) \rangle \quad (38)$$

and $|\{q, n\}\rangle$ represents an eigenstate of the positions $\{q_i\}$ and fermion occupation numbers $\{n_i\}$ at each site. In this representation,

$$H = H_0 + H_1 \quad (39)$$

where

$$H_1 = -\tilde{t} \sum_i \left(c_i^\dagger c_{i+1} + c_{i+1}^\dagger c_i \right) \quad (40)$$

is the fermion hopping term, and

$$H_0 = - \sum_i \frac{\partial^2}{\partial q_i^2} + V(\{q, n\}) \quad (41)$$

with

$$V(\{q, n\}) = \sum_i q_i^2 - \tilde{g} \sum_i q_i \left(n_i - \frac{1}{2} \right) \quad (42)$$

as the ‘‘potential’’ term.

The evolution equation (35) now has the form of a diffusion equation in configuration space. It is assumed that the ground-state wave function can be chosen positive everywhere, and it is simulated by the density distribution of an ensemble of random walkers in configuration space, whose time evolution mimics that of equation (36).

To obtain good accuracy, one needs to introduce some *variational guidance*, which can be done as follows. Let $|\Psi_T\rangle$ be a trial vector, e.g., some variational approximation to the true ground-state eigenvector with wave function:

$$\Psi_T(\{q, n\}) = \langle \{q, n\} | \Psi_T \rangle. \quad (43)$$

Then carry out a similarity transformation

$$|\Phi(\tau)\rangle \rightarrow |\Phi'(\tau)\rangle = \Psi_T |\Phi(\tau)\rangle \quad (44)$$

$$H \rightarrow H' = \Psi_T H \Psi_T^{-1} \quad (45)$$

where the transformation matrix Ψ_T is diagonal in $\{q, n\}$ space, with diagonal entries $\Psi_T(\{q, n\})$. The modified evolution equation will be

$$|\Phi'(\tau + \Delta\tau)\rangle = \exp(\Delta\tau(E_T - H')) |\Phi'(\tau)\rangle \quad (46)$$

Let us now separate the fermion hopping term from the rest of the Hamiltonian, and write for small $\Delta\tau$

$$\exp(\Delta\tau(E_T - H')) \simeq \exp(\Delta\tau(E_T - H'_0)) [1 - \Delta\tau H'_1] + O(\Delta\tau^2) \quad (47)$$

(All our calculations from here on will only be accurate to $O(\Delta\tau)$).

Now H_0 transforms to

$$\begin{aligned} H'_0 &= \Psi_T \left[- \sum_i \frac{\partial^2}{\partial q_i^2} + V(\{q, n\}) \right] \Psi_T^{-1} \\ &= - \sum_i \left[\frac{\partial^2}{\partial q_i^2} + 2\Psi_T \left(\frac{\partial \Psi_T^{-1}}{\partial q_i} \right) \frac{\partial}{\partial q_i} + \Psi_T \left(\frac{\partial^2 \Psi_T^{-1}}{\partial q_i^2} \right) \right] + V(\{q, n\}) \\ &= \Psi_T^{-1} H_0 \Psi_T + \sum_i \left[p_i^2 + 2ip_i \left(\Psi_T^{-1} \frac{\partial \Psi_T}{\partial q_i} \right) \right] \end{aligned} \quad (48)$$

as shown by Chin, Negele, and Koonin³⁹ where the operator $p_i = -i\frac{\partial}{\partial q_i}$ acts on everything to the right of it as usual. Then the matrix element between position eigenstates corresponding to the time-step $\Delta\tau$ at iteration m can be written³⁹

$$\begin{aligned} & \langle \{q, n\}^{(m+1)} | \exp(\Delta\tau(E_T - H'_0)) | \{q, n\}^{(m)} \rangle \\ & \simeq \frac{1}{(4\pi\Delta\tau)^{N/2}} \exp\left(-\frac{1}{4\Delta\tau} \sum_i [q_i^{(m+1)} - q_i^{(m)} - 2\Delta\tau\Psi_T^{-1} \frac{\partial\Psi_T}{\partial q_i}]^2 - \Delta\tau[\Psi_T^{-1}(H_0\Psi_T) - E_T]\right) \\ & + O(\Delta\tau^2) \end{aligned} \quad (49)$$

Representing the wave function Φ' by a distribution of random walkers in position space, the Monte Carlo simulation proceeds as follows. Each iteration corresponds to a time step $\Delta\tau$, and involves a sweep through each site in turn. The first term in the exponential (49) is simulated by a displacement of each position variable

$$\Delta q_i = 2\Delta\tau\Psi_T^{-1} \frac{\partial\Psi_T}{\partial q_i} + \chi \quad (50)$$

where χ is randomly chosen from a Gaussian distribution with standard deviation $\sqrt{2\Delta\tau}$. The first term in (50) is the “drift” term, and the second is the “diffusion” term. The second term in the exponential (49) is simulated by multiplying the “weight” of each walker by an equivalent amount.

We also need to simulate the fermion hopping term:

$$\begin{aligned} & \langle \{q, n\}^{(m+1)} | [1 - \Delta\tau H'_1] | \{q, n\}^{(m)} \rangle \\ & = \frac{\Psi_T(\{q, n\}^{(m+1)})}{\Psi_T(\{q, n\}^{(m)})} \langle \{q, n\}^{(m+1)} | [1 + \tilde{t}\Delta\tau \sum_i (c_i^\dagger c_{i+1} + c_{i+1}^\dagger c_i)] | \{q, n\}^{(m)} \rangle \end{aligned} \quad (51)$$

The factor in front produces a “reweighting” of the walkers in the ensemble; while the hopping term itself produces new configurations on walkers with different fermion occupation numbers.

At the end of each iteration, the trial energy E_T is adjusted to compensate for any change in the total weight of all walkers in the ensemble; and a “branching” process is carried out, so that walkers with weight greater than (say) 2 are split into two new walkers, while any two walkers with weight less than (say) 0.5 are combined into one; chosen randomly according to weight from the originals. This procedure of “Runge smoothing”⁴³ maximises statistical accuracy by keeping the weights of all walkers within fixed bounds, while minimizing any fluctuations in the total weight due to the branching process. When equilibrium is reached after many sweeps through the lattice, the average value of the trial energy E_T will give an estimate of the ground-state energy E_0 , from equation (37); and the density of the ensemble in configuration space will be proportional to $\Phi_0\Psi_T$. Various corrections due to the finite time interval $\Delta\tau$ have been ignored in this discussion, and the limit $\Delta\tau \rightarrow 0$ must be taken in some fashion to eliminate such corrections.

As a trial wave function, we choose a Gaussian, displaced by an amount q_0 at each site depending whether the site is occupied or unoccupied:

$$\Psi_T(\{q, n\}) = \exp\left[-c \sum_i (q_i - 2q_0(n_i - \frac{1}{2}))^2\right] \quad (52)$$

where c and q_0 are variational parameters. Then the local “trial energy”

$$E_L(\{q, n\}) \equiv \Psi_T^{-1} H_0 \Psi_T = \sum_i [q_i^2 - \tilde{g}q_i(n_i - \frac{1}{2})] - \sum_i [4c^2(q_i - 2q_0(n_i - \frac{1}{2}))^2 - 2c] \quad (53)$$

and the “drift” term is

$$2\Psi_T^{-1} \frac{\partial\Psi_T}{\partial q_i} = -4c(q_i - 2q_0(n_i - \frac{1}{2})) \quad (54)$$

while the “reweighting factor” in equation (51) is

$$\frac{\Psi_T(\{q, n\}^{(m+1)})}{\Psi_T(\{q, n\}^{(m)})} = \exp\left[4cq_0 \sum_i q_i(n_i^{(m+1)} - n_i^{(m)})\right] \quad (55)$$

If the choice of trial function is a good one, and E_T is adjusted to approximately equal E_0 , then we will have

$$E_L \simeq E_T \simeq E_0 \quad (56)$$

so that the weight of each walker changes very little at each time step, according to equation (51), so that the fluctuations in the weights are small, and consequently the accuracy of the calculation is maximised.

B. Expectation Values

Ground-state expectation values can also be measured, using a “secondary amplitude” technique discussed by Hamer *et al.*^{36,41,42}. Let $\langle Q \rangle_0$ be the expectation value to be measured, where we assume the operator Q is diagonal in the $\{q, n\}$ representation. Use Q as a perturbation to the Hamiltonian:

$$H' = H + xQ. \quad (57)$$

Let $E'_0(x)$ denote the ground state expectation value of this Hamiltonian. By the Hellmann-Feynman theorem, the required expectation value is given by

$$\langle Q \rangle_0 = \left. \frac{dE'_0}{dx} \right|_{x=0}. \quad (58)$$

Taylor expand the eigenvector and eigenvalue

$$|\Phi(\tau, x)\rangle = |\Phi^0(\tau)\rangle + x|\Phi^1(\tau)\rangle + O(x^2) \quad (59)$$

$$E'_0(x) = E_0 + xE^1 + O(x^2) \quad (60)$$

substitute in the evolution equation (36) (ignoring any variational guidance for the time being), and equate powers of x to obtain:

$$|\Phi^0(\tau + \Delta\tau)\rangle = \exp(\Delta\tau(E_T - H))|\Phi^0(\tau)\rangle \quad (61)$$

and

$$|\Phi^1(\tau + \Delta\tau)\rangle = \exp(\Delta\tau(E_T - H))|\Phi^1(\tau)\rangle + \Delta\tau(E^1 - Q)|\Phi^0(\tau)\rangle. \quad (62)$$

Equation (61) is just the original evolution equation (36) for the unperturbed system. Equation (62) is an evolution equation of similar structure for the first-order wave function $|\Phi^1\rangle$. It is simulated by giving a “secondary” weight to each walker in the ensemble, and evolving it according to (62); while a secondary trial energy E'_T is used to estimate E^1 , and is adjusted after each iteration to compensate for any change in the total of all secondary weights. At equilibrium, the average value of E'_T gives an estimate of E^1 , which is equivalent to $\langle Q \rangle_0$ by equation (58).

V. RESULTS AND DISCUSSION

GFMC runs were performed for a range of different couplings g/ω at hopping parameter values $t = 0.1\omega, \omega$ and 10ω , for lattice sizes of 2, 4, 6, 8, and 16 sites. In each case, the variational parameters c and q_0 (compare equation (52)) were adjusted to their optimum values by a series of trial runs. Production runs typically employed an ensemble of 2000 walkers for 20,000 iterations. The first 2000 iterations were discarded to allow for equilibrium, and the remainder were averaged over blocks of 1024 iterations before estimating the error to minimize correlation effects. Calculations were performed on a cluster of six HP735 workstations. A typical run for 16 sites took 1-2 hours of CPU time. Two different time steps were used in each case, namely $\Delta\tau = 0.005$ and 0.01 at $t = 0.1\omega$, $\Delta\tau = 0.0005$ and 0.001 at $t = \omega$, and $\Delta\tau = 0.001$ and 0.002 at $t = 10\omega$. The results were then linearly extrapolated to $\Delta\tau = 0$.

The quantities measured were the ground-state energy (in the half-filled sector), $E_0(N)$, the energy gap (to the ‘‘one hole’’ sector with one fewer fermions), $E_{-1}(N) - E_0(N)$, and ground-state expectation values for the mean displacement $\langle q_i(2n_i - 1) \rangle$, the mean square displacement $\langle q_i^2 \rangle$, and two correlated fermion expectation values, $\langle n_i n_{i+N/2} \rangle$ and $\langle n_i n_{i-1+N/2} \rangle$, where N is the lattice size. The difference between these last two values provides an estimate of the amount of ‘‘staggering,’’ or dimerization, in the fermion occupation numbers. (Compare equation (65) below). A sample of results is shown in Table I.

The charge velocity u_ρ was extracted from a finite size scaling plot of the ground state energy per site $E_0(N)/N$ versus $1/N^2$ (compare Figure 1). According to equation (10) this should be a straight line for large N . To allow for the small curvature of our plots, because we used only moderately large system sizes ($N = 2, 4, 6, 8,$ and 16 sites), the data was fitted to

$$\frac{E_0(N)}{N} = \epsilon_\infty - \frac{\pi u_\rho}{6N^2} + \frac{a}{N^4}. \quad (63)$$

The correction-to-scaling term $O(N^{-4})$ matches that predicted to hold for the XXZ model^{31,32}, at least for weak interactions (i.e., small μ). For stronger interactions the exponent is interaction dependent. At the metal-insulator transition the correction-to-scaling term is $O((N \ln N)^{-2})$. However, we found that using such a form did not improve the quality of the least square fits near the transition.

For free fermions ($g = 0$) the values of ϵ_∞ and u_ρ extracted from the fits were found to agree well with the known analytic results $\epsilon_\infty = -2t/\pi$ and $u_\rho = 2t$ (Table II). For $t = 0.1\omega$ the dependence of the ground state energy on the coupling is in good agreement with small polaron theory (Figure 3).

The energy gap Δ of the infinite system was extracted from finite size scaling plots of the hole energy $E_{-1}(N) -$

$E_0(N)$ versus $1/N$ (compare Figure 2). To allow for the corrections to scaling this was fitted to

$$E_{-1}(N) - E_0(N) = \Delta + \frac{\pi u_\rho}{2K_\rho} \frac{1}{N} + \frac{b}{N^3}. \quad (64)$$

Again, the higher order term $O(N^{-3})$ was chosen to be consistent with known results for free fermions and the XXZ model with weak interactions. To extract K_ρ we need to use the value of u_ρ extracted earlier. (Strictly speaking equation (64) is only valid when $\Delta = 0$ but we use Δ as a parameter in our fits to check that we are in the critical regime. Also, the derivation of equation (64) requires particle-hole symmetry, i.e., $E_{-1}(N) = E_{+1}(N)$. We checked for several parameter values that the Monte Carlo results were consistent with this.)

Figure 4 (a) shows the dependence of the charge velocity u_ρ on the fermion-phonon coupling g for $t = 0.1\omega$. The results are in good agreement with equations (20) and (23) (solid line in Figure 4(a)). The charge velocity is significantly reduced by polaronic band narrowing. The correlation exponent K_ρ is shown in Figure 4 (b) as a function of the fermion phonon coupling. The dependence of K_ρ on the coupling is consistent with the metallic phase being a Luttinger liquid. The fact $K_\rho < 1$ indicates repulsive interactions in the Luttinger liquid. K_ρ is not plotted for $g > 1.5\omega$ because the relative error is very large. This is because its determination depends on the value of u_ρ which has a very large relative error for $g > 1.5\omega$ (see Figure 4 (a)). For $t = 0.1\omega$, equations (20) and (21), for the small polaronic model together with the criterion $V = 2J$ can be used to determine that the transition from the Luttinger liquid to the insulating phase occurs when $g = 2.075\omega$.

The charge-density-wave order parameter m_e , defined by (2), must be zero for any finite size system. However, in the dimerized phase we also have for j large

$$\langle n_i n_{i+j} \rangle = \frac{1}{4} + (-1)^j m_e^2 \quad (65)$$

and so

$$m_e^2 = \frac{1}{2} | \langle n_i n_{i+N/2} \rangle - \langle n_i n_{i-1+N/2} \rangle |. \quad (66)$$

This equation was used to determine m_e^2 from the results for $N = 16$ sites.

Figure 5 (a) shows the coupling constant dependence of m_e^2 for $t = 0.1\omega$. The quantum Monte Carlo data suggests there is a transition near $g = 1.8\omega$. This is consistent with the small polaron theory prediction of $g = 2.075\omega$ since the latter theory is only valid to order $1/\lambda \sim \pi t \omega / g^2$, i.e., about 10%. Figure 5 (b) shows the energy gap as a function of coupling. It is not possible to detect the transition in the energy gap data. Small polaron theory predicts an energy gap smaller than typical uncertainties in the Monte Carlo data.

Figure 6 shows the coupling strength dependence of the mean lattice displacement $\langle q_i(2n_i - 1) \rangle$ and the mean

square lattice displacement $\langle q_i^2 \rangle$ for $t = 0.1\omega$ and a system of 16 sites. The results are very close to those anticipated for localized fermions (compare equations (16) and (17)). For $t = \omega$ and $t = 10\omega$ the mean lattice displacement was also non-zero, i.e., the ground state was polaronic for all couplings, although the magnitude of the displacement decreased significantly with increasing t . Similar trends are seen for the Holstein model on two sites⁴⁴.

For $t = \omega$ the charge velocity is again reduced by polaronic effects (Figure 7 (a)) but not by as much as for $t = 0.1\omega$. The interactions in the Luttinger liquid are now attractive ($K_\rho > 1$). Both the order parameter and the energy gap show a transition to the insulating phase near $g = 1.7\omega$ (Figure 8). Clearly our results are inconsistent with the universal value $K_\rho = 1/2$ expected for a Kosterlitz-Thouless transition^{33,34}.

For $t = 10\omega$ the charge velocity decreases by less than ten per cent with increasing g/ω (Figure 9). This is in contrast to the cases of $t = 0.1\omega$ and $t = \omega$ for which the charge velocity decreases by about an order of magnitude. The correlation function exponent K_ρ increases by about fifty per cent. As for $t = \omega$, $K_\rho \neq 1/2$ at the transition and so the transition cannot be a Kosterlitz-Thouless transition. The order parameter m_e and energy gap Δ become nonzero about $g = 3.5\omega$ (Figure 10). This is quite different from what is anticipated by Hirsch and Fradkin⁹. They performed simulations from $t = 0.5\omega$ up to $t = 3.1\omega$. They found a smooth decrease in the critical value of $\lambda_c = g_c^2/\pi\omega t$ with increasing t/ω , and anticipated a smooth crossover to $\lambda_c = 0$ for $\omega = 0$. Extrapolating their results to $t = 10\omega$ gives $\lambda_c \sim 0.01$ and $g_c \sim 0.6\omega$ compared to our value of $g_c \simeq 3.5\omega$. Note that the ratio of the energy gap to its mean field value (Figure 10 (b)) is much smaller than the ratio of the charge-density-wave order parameter to its mean field value. This is consistent with work showing that the zero point motion of the lattice can reduce the magnitude of the order parameter by a small amount but produce a substantial subgap tail in the fermionic density of states⁵. (For example, results on the continuum version of the SSH model shown in Figures 1 and 3 of Reference⁵ show that for one set of parameter values the energy gap can be about 60 % of the mean-field value while the order parameter is only reduced by about 5 %).

The phase boundary as a function of t/ω and g/ω between the metallic and insulating phases is shown in Figure 11. The solid curve is the boundary predicted by small polaron theory and the XXZ model (Section III B). This curve is only shown for $t < \omega$ since this model is only valid in the strong coupling limit ($t \ll g^2/\omega$). The crosses are the boundary points deduced from Figures 5, 8, and 10. It should be stressed that there is some ambiguity in determining the phase boundary. According to mean-field theory the transition occurs at $g = 0$ but the solid curves in Figures 8 and 10 suggest that the transition is actually only detectable at $g \sim 0.6\omega$ and $g \sim 2\omega$, respectively. On the other hand, for $t = 0.1\omega$ small po-

laron theory and the XXZ model predict a Kosterlitz-Thouless transition at $g = 2.075\omega$ and the solid curve in Figure 5 (a) shows there is very little ambiguity associated with this transition point. For comparison the boundary points found by Hirsch and Fradkin⁹ (Figure 11 in their paper) are also shown. For $t = \omega$ there is a discrepancy between our results and theirs: they observe the transition at smaller coupling than we do. We have no explanation for this discrepancy.

VI. CONCLUSIONS

We have shown that the Green's function Monte Carlo technique can be successfully used to investigate a one dimensional fermion-phonon model. As far as we are aware this is the first application of this technique to this important class of models. The results were of sufficiently high precision that a finite size scaling analysis of the results could be performed. For the case of free fermions ($g = 0$) and the strong coupling limit ($g^2 \gg t\omega$) our results agree with known analytic results.

Our results are consistent with the following physical picture of the Holstein model of spinless fermions at half-filling. For sufficiently weak coupling the system is in a metallic, i.e., gapless phase, with the properties of a Luttinger liquid, i.e., the exponents associated with the decay of correlation functions depend on the coupling strength. The fermions are polaronic, i.e., there is a finite phonon displacement q_e associated with the occupation of a site by a fermion and the velocity of excitations, u_ρ , is reduced below the free electron value $2t$. As the coupling g increases and t/ω decreases q_e increases and u_ρ (which is a measure of the polaronic band width) decreases. Qualitatively similar behaviour is seen for the two-site Holstein model⁴⁴. In the anti-adiabatic limit ($t \ll \omega$) the effective interaction between polarons is repulsive and for strong coupling the Holstein model can be mapped onto the XXZ antiferromagnetic spin chain (Section III B). However, as t/ω increases the effective interaction becomes attractive. This is indicated by a change in the value of the stiffness constant K_ρ from values less than one to values larger than one. When the fermion-phonon coupling is sufficiently large the system undergoes a transition to an insulating phase, i.e., an energy gap opens at the Fermi surface. There is long-range charge-density-wave order and a dimerization of the phonons in this phase. Our results for $t = \omega$ and $t = 10\omega$ are inconsistent with the metal-insulator transition being infinite order. On the other hand we do not see any evidence of the first-order transition suggested by Zheng, Feinberg, and Avignon¹¹ and by Wu, Huang, and Sun¹² for certain parameter values.

This work suggests several possible future investigations which we plan to pursue: (a) The adiabatic region of the phase diagram ($t \gg \omega$), in which we found a larger region of the metallic phase than anticipated by

Hirsch and Fradkin, needs to be investigated further. (b) The relative importance of superconducting and charge-density-wave correlations should be investigated in the region of the metallic phase for which the effective interactions are attractive. (c) Alternative variational wavefunctions, such as the double Gaussian proposed by Shore and Sander²³, could be used instead of the single Gaussian (52) used for the variational guidance. Finally, we plan to use this method to investigate the Holstein model with spin, and away from half-filling, as well as the Su-Schrieffer-Heeger model, and the spin-Peierls problem.

ACKNOWLEDGMENTS

Work at UNSW was supported by the Australian Research Council. We thank J. Voit for a critical reading of the manuscript and many helpful suggestions. We thank M. Gulacsi, J. Oitmaa, and R. Singh for helpful discussions. Computer time was provided by the Centre for Advanced Numerical Computation in Engineering and Science (CANCES) at UNSW.

* electronic address: ross@newt.phys.unsw.edu.au

¹ G. Grüner, *Density Waves in Solids*, (Addison-Wesley, Redwood City, 1994).

² R. Peierls, *Quantum Theory of Solids*, (Oxford, 1955), p. 108.

³ T. Holstein, *Ann. Phys.* **8**, 325, 343 (1959).

⁴ A. J. Heeger, S. Kivelson, J.R. Schrieffer, and W.P. Su, *Rev. Mod. Phys.* **60**, 781 (1988).

⁵ R. H. McKenzie and J. W. Wilkins, *Phys. Rev. Lett.* **69**, 1085 (1992), and references therein.

⁶ K. Kim, R. H. McKenzie, and J. W. Wilkins, *Phys. Rev. Lett.* **71**, 4015 (1993).

⁷ F. H. Long, S. P. Love, B. I. Swanson, and R. H. McKenzie, *Phys. Rev. Lett.* **71**, 762 (1993); L. Degiorgi, St. Thieme, B. Alavi, G. Grüner, R.H. McKenzie, K. Kim, and F. Levy, *Phys. Rev. B* **52**, 6203 (1995), and references therein.

⁸ W. P. Su, *Solid State Comm.* **42**, 497 (1982); E. Fradkin and J. E. Hirsch, *Phys. Rev. B* **27**, 1680 (1983); D. Schmeltzer, R. Zeyher, and W. Hanke, *Phys. Rev. B* **33**, 5141 (1986); A. Auerbach and S. Kivelson, *Phys. Rev. B* **33**, 8171 (1986); Z. B. Su, Y. X. Wang, and L. Yu, *Commun. Theor. Phys.* (Beijing) **6**, 313 (1986); J. Yu, H. Matsuoaka, and W. P. Su, *Phys. Rev. B* **37**, 10367 (1988); G. C. Psaltakis and N. Papanicolaou, *Solid State Comm.* **66**, 87 (1992); A. Takahashi, *Phys. Rev. B* **46**, 11550 (1992); H. Zheng, *Phys. Rev. B* **50**, 6717 (1994); C. Q. Wu, Q. F. Huang, and X. Sun, *Phys. Rev. B* **52**, 7802 (1995).

⁹ J. E. Hirsch and E. Fradkin, *Phys. Rev. B* **27**, 4302 (1983). To compare our results with theirs set $K = M\omega^2$ and $\lambda = g(2M\omega)^{1/2}$.

- ¹⁰ C. Bourbonnais and L. G. Caron, *J. Phys. France* **50**, 2751 (1989).
- ¹¹ H. Zheng, D. Feinberg, and M. Avignon, *Phys. Rev. B* **39**, 9405 (1988).
- ¹² C. Q. Wu, Q. F. Huang, and X. Sun, *Phys. Rev. B* **52**, 15683 (1995).
- ¹³ J. Voit and H. J. Schulz, *Phys. Rev.* **36** 968, (1987).
- ¹⁴ J. R. Freericks, M. Jarrell, and D. J. Scalapino, *Phys. Rev. B* **48**, 6302 (1993), and references therein.
- ¹⁵ P. Niyaz, J. E. Gubernatis, R. T. Scalettar, and C. Y. Fong, *Phys. Rev. B* **48**, 16011 (1993), and references therein.
- ¹⁶ F. Marsiglio, *Physica C* **244**, 21 (1995).
- ¹⁷ A. S. Alexandrov, V. V. Kabanov, and D. K. Ray, *Phys. Rev. B* **49**, 9915 (1994), and references therein.
- ¹⁸ J. Voit, *Rep. Prog. Phys.* **58**, 977 (1995).
- ¹⁹ M. J. Rice and E. J. Mele, *Phys. Rev. B* **25**, 1339 (1982).
- ²⁰ M. Hase, I. Terasaki, and K. Uchinokura, *Phys. Rev. Lett.* **70**, 3651 (1993), and references therein.
- ²¹ E. Fradkin, *Field Theories of Condensed Matter Systems* (Addison Wesley, Redwood City, 1991).
- ²² G. Benfatto, G. Gallavotti, and J. L. Lebowitz, *Helv. Phys. Acta* **68**, 312 (1995).
- ²³ H. B. Shore and L. M. Sander, *Phys. Rev. B* **7**, 4537 (1973).
- ²⁴ B. Gerlach and H. Löwen, *Rev. Mod. Phys.* **63** 63 (1991).
- ²⁵ F. D. M. Haldane, *Phys. Rev. Lett.* **45**, 1358 (1980).
- ²⁶ J. Voit, *J. Phys. Cond. Matter* **5**, 8305 (1993).
- ²⁷ I. Affleck, *Phys. Rev. Lett.* **56**, 746 (1986); H. W. J. Blöte, J. L. Cardy, and M. P. Nightingale, *Phys. Rev. Lett.* **56**, 742 (1986).
- ²⁸ J. L. Cardy, *J. Phys. A* **17**, L385 (1984).
- ²⁹ G. D. Mahan, *Many-Particle Physics*, Second edition, (Plenum, New York, 1990) p.285ff.
- ³⁰ Similar calculations were made by G. Beni, P. Pincus, and J. Kanamori [*Phys. Rev. B* **10**, 1896 (1974)] for the case of electrons with spin.
- ³¹ C. N. Yang and C. P. Yang, *Phys. Rev.* **150**, 321, 327 (1966).
- ³² C. J. Hamer, *J. Phys. A* **19**, 3335 (1986).
- ³³ R. Shankar, *Int. J. Mod. Phys. B* **4**, 2371 (1990).
- ³⁴ T. Giamarchi, *Phys. Rev. B* **44**, 2905 (1991).
- ³⁵ R. J. Baxter, *Exactly Solved Models in Statistical Mechanics* (Academic, London, 1982).
- ³⁶ P. F. Price, C. J. Hamer and D. O'Shaughnessy, *J. Phys. A* **26**, 2855 (1993).
- ³⁷ D. M. Ceperley and M. H. Kalos, in "Monte Carlo Methods in Statistical Mechanics," ed. K. Binder (Springer-Verlag, New York, 1979), p.145.
- ³⁸ M. H. Kalos, D. Levesque and L. Verlet, *Phys. Rev. A* **9**, 2178 (1974).
- ³⁹ S. A. Chin, J. W. Negele, and S. E. Koonin, *Ann. Phys.* (N.Y.) **157**, 140 (1984).
- ⁴⁰ D. W. Heys and D. R. Stump, *Phys. Rev. D* **28**, 2067 (1983).
- ⁴¹ C. J. Hamer, K. C. Wang, and P. F. Price, *Phys. Rev. D* **50**, 4693 (1994).
- ⁴² C. J. Hamer, M. Sheppard, Z. Weihong, and D. Schütte, submitted to *Phys. Rev. D*.
- ⁴³ K. J. Runge, *Phys. Rev. B* **45**, 7229 (1992).
- ⁴⁴ M. Sonnek, T. Frank, and M. Wagner, *Phys. Rev. B* **49**, 15637 (1994).

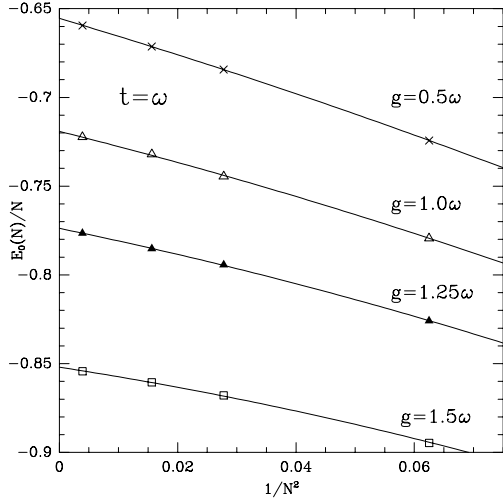


FIG. 1. Finite-size scaling of the ground state energy $E_0(N)$ for different values of the fermion-phonon coupling g . The data shown are for $N = 4, 6, 8,$ and 16 lattice sites. All data are for a fermion hopping parameter t equal to the phonon frequency ω and for a half-filled band (i.e., one fermion per two sites). All energies are in units of ω . If the system is critical for a particular g value then the data for N large should lie on a straight line (see equation (10)). The lines are least square fits to a parabola (see text). The errors in the Monte Carlo data are smaller than the symbol sizes.

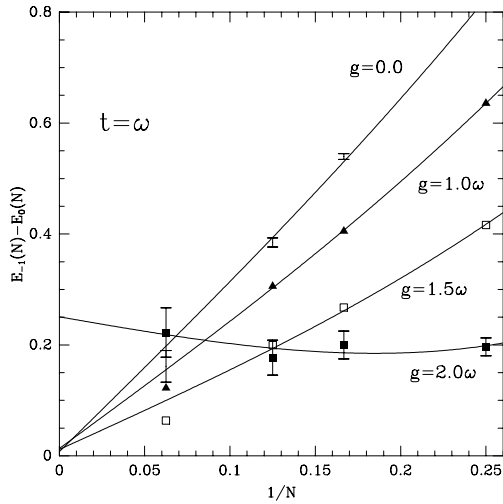


FIG. 2. Finite-size scaling of the hole energy for different values of the fermion-phonon coupling g . The data shown are for $N = 4, 6, 8,$ and 16 lattice sites. $E_0(N)$ is the ground state energy of a system of $N/2$ fermions and $E_{-1}(N)$ is the ground state energy of a system of $N/2 - 1$ fermions. All data are for a fermion hopping parameter t equal to the phonon frequency ω . All energies are in units of ω . If the system is critical then for that g value the data for large N should lie on a straight line through the origin (see equation (11)). The lines are least square fits to a cubic (see text).

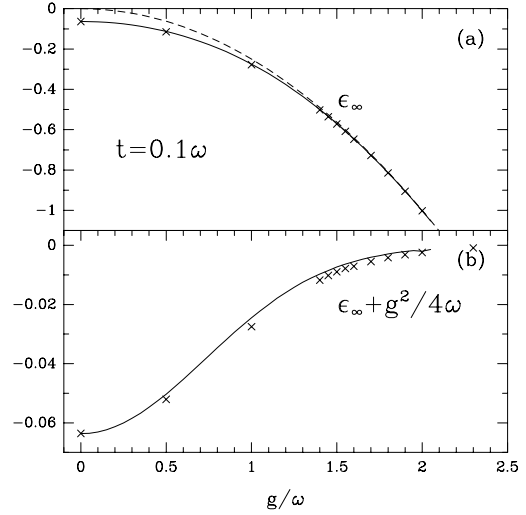


FIG. 3. Dependence of the ground state energy per site ϵ_∞ on the fermion-phonon coupling g for $t = 0.1\omega$. The solid lines are the predictions of the small polaron model (Section III B). The error bars are smaller than the symbol size. All energies are in units of ω . (a) ϵ_∞ is deduced from the intercept of the finite-size scaling plot of the ground state energy (compare Figure 1). The dashed line is the polaron binding energy $-g^2/4\omega$ and clearly represents almost all of the ground state energy. (b) The polaron binding energy has been subtracted from the ground state energy to make a more accurate comparison with small polaron theory.

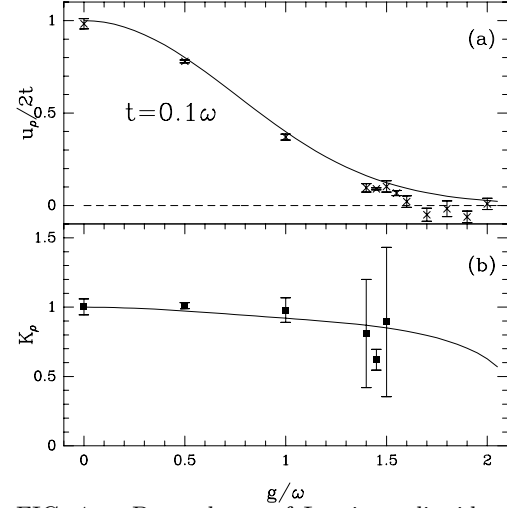


FIG. 4. Dependence of Luttinger liquid parameters on the fermion-phonon coupling g for $t = 0.1\omega$. The solid lines are the predictions of the small polaron model (Section III B). (a) The velocity of charge excitations u_ρ is deduced from the slope of the finite-size scaling plot of the ground state energy (compare Figure 1) and is normalized by the free fermion value $2t$. The decrease of u_ρ with increasing g is due to the narrowing of the bandwidth by polaronic effects. (b) The correlation function exponent K_ρ is deduced from the ratio of the slopes of the finite-size scaling plots in Figures 1 and 2 (see equation (11)). The error bars are based on the uncertainties in the least-squares fits to the finite size scaling data (compare figures 1 and 2).

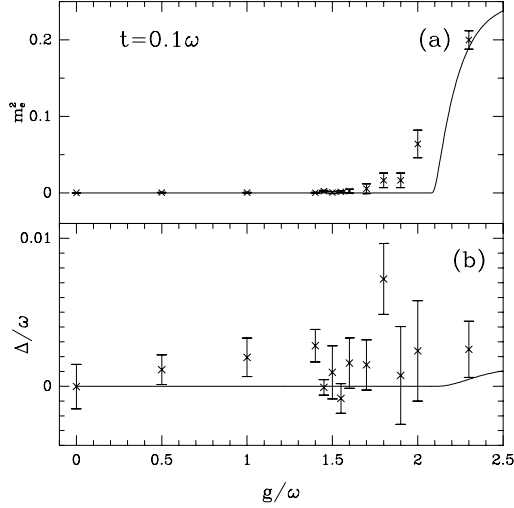


FIG. 5. Dependence on the fermion-phonon coupling g of (a) the square of the charge-density-wave order parameter m_e and (b) the energy gap Δ . The solid lines are the predictions of the small polaron model (Section III B). It predicts an infinite order transition at $g = 2.075\omega$. m_e^2 was deduced from equation (66) for a system of 16 sites. The energy gap was deduced from the $N = \infty$ extrapolation of the finite size scaling plot of the hole energy (compare Figure 2). Both the order parameter and the energy gap become non-zero for $g > 1.8$ marking the transition into the insulating phase.

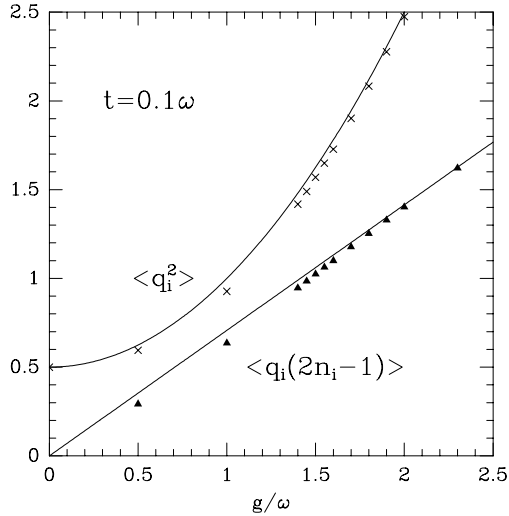


FIG. 6. Dependence on the fermion-phonon coupling g of the mean lattice displacement $\langle q_i(2n_i - 1) \rangle$ and the mean square lattice displacement $\langle q_i^2 \rangle$ for $t = 0.1\omega$ and a system of 16 sites. The displacements are in units of $(M\omega)^{-1/2}$. The solid lines are the predictions for localized fermions (Section III A).

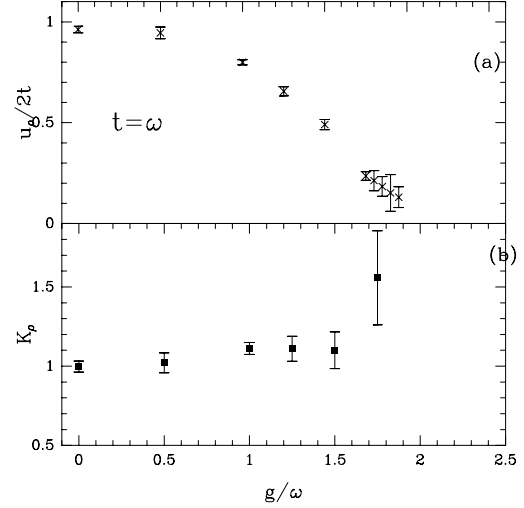


FIG. 7. Same as Figure 4 but with $t = \omega$. The fact that K_ρ depends on g and is larger than one is consistent with the metallic phase being a Luttinger liquid with attractive interactions. If the metal-insulator transition was Kosterlitz-Thouless K_ρ would equal 0.5 at the transition.

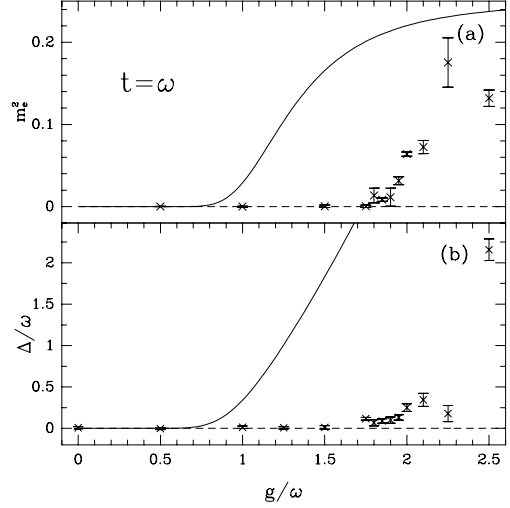


FIG. 8. Same as Figure 5 but with $t = \omega$. The solid curves are the predictions of mean field theory (Section III D).

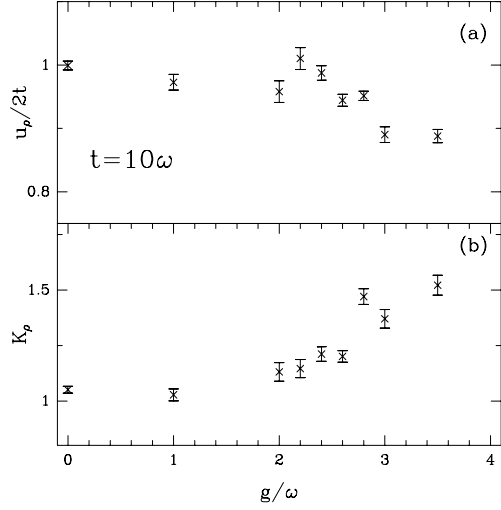


FIG. 9. Same as Figure 4 but with $t = 10\omega$. Note that the vertical scale is expanded compared to Figures 4 and 7. Since $K_\rho \neq 0.5$ near the transition the transition is not Kosterlitz-Thouless.

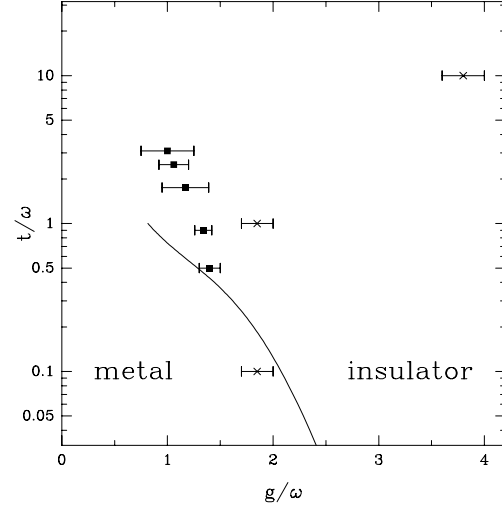


FIG. 11. Phase diagram showing the boundary between the metallic and insulating phase. The solid curve is the prediction of small polaron theory and the XXZ model (Section III B). The crosses are the results of this study and the solid squares the results of Hirsch and Fradkin⁹.

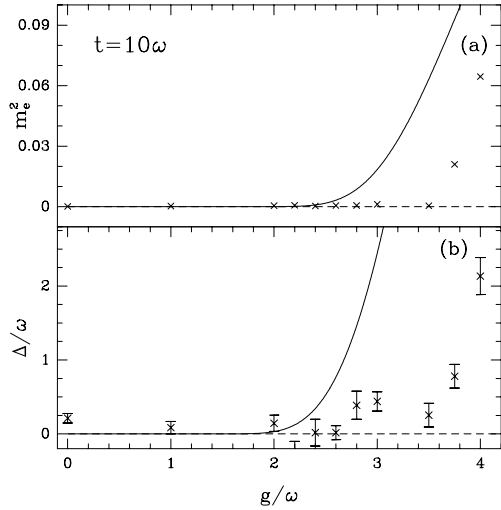


FIG. 10. Same as Figure 5 but with $t = 10\omega$. The solid curves are the predictions of mean field theory (Section III D).

TABLE I. Monte Carlo results for different quantities for $t = \omega$ and $g = 1.5\omega$ and for various system sizes. The energies are in units of ω and displacements in units of $(M\omega)^{-1/2}$.

N	$E_0(N)/N$	$E_{-1}(N) - E_0(N)$	$\langle q_i(2n_i - 1) \rangle$	$\langle q_i^2 \rangle$	$\langle n_i n_{i+M/2} \rangle$	$\langle n_i n_{i-1+M/2} \rangle$
2	-1.143 ± 0.001	1.158 ± 0.004	0.313 ± 0.005	0.748 ± 0.008	0.000 ± 0.000	0.500 ± 0.000
4	-0.895 ± 0.001	0.416 ± 0.004	0.446 ± 0.001	0.864 ± 0.004	0.260 ± 0.001	0.120 ± 0.0004
6	-0.868 ± 0.001	0.268 ± 0.009	0.470 ± 0.005	0.883 ± 0.007	0.217 ± 0.001	0.244 ± 0.001
8	-0.861 ± 0.002	0.200 ± 0.015	0.484 ± 0.002	0.902 ± 0.003	0.240 ± 0.002	0.229 ± 0.001
16	-0.854 ± 0.001	0.064 ± 0.027	0.488 ± 0.004	0.904 ± 0.005	0.247 ± 0.002	0.246 ± 0.002

TABLE II. Comparison of Monte Carlo results with known results for free fermions. The ground state energy per site of the infinite system, ϵ_∞ , and the velocity of charge excitations, u_ρ , are normalised to their free fermion values. The correlation exponent K_ρ is one for free fermions.

$\frac{t}{\omega}$	$\frac{\pi\epsilon_\infty}{2t}$	$\frac{u_\rho}{2t}$	K_ρ
0.1	0.999 ± 0.001	0.98 ± 0.03	1.00 ± 0.06
1	1.000 ± 0.001	0.96 ± 0.02	1.00 ± 0.04
10	0.999 ± 0.003	1.00 ± 0.01	0.95 ± 0.02